Morphological and Physicochemical Characterization of Single-Species Bacterial Biofilms Probed by SEM, FTIR-ATR, and μ-Raman Techniques

GIUSEPPE PALADINI[1], FRANCESCO CARIDI[1], DOMENICO MAJOLINO[1],
VALENTINA VENUTI[1], PAOLA CARDIANO[2], FEDERICA DE GAETANO[2],
GABRIELE LANDO[2], ROSANNA STANCANELLI[2], SILVANA TOMMASINI[2],
CINZIA ANNA VENTURA[2], BARBARA FAZIO[3], CINZIA LOMBARDO[4], MARIO SALMERI[4],
VENERANDO PISTARÀ'[5]

[1]Dipartimento di Scienze Matematiche e Informatiche, Scienze Fisiche e Scienze della Terra,
Università degli Studi di Messina,
Viale Ferdinando Stagno D'Alcontres 31, I-98166 Messina,
ITALY

[2]Dipartimento di Scienze Chimiche, Biologiche, Farmaceutiche ed Ambientali,
Università degli Studi di Messina,
Viale Ferdinando Stagno D'Alcontres 31, I-98166 Messina,
ITALY

[3]URT LabSens, CNR-DSFTM Messina, c/o Dipartimento di Scienze Chimiche, Biologiche,
Farmaceutiche ed Ambientali,
Università degli Studi di Messina,
Viale Ferdinando Stagno D'Alcontres 31, I-98166 Messina,
ITALY

[4]Dipartimento di Scienze Biomediche e Biotecnologiche,
Università degli Studi di Catania,
Torre Biologica, Via Santa Sofia 97, I-95123 Catania,
ITALY

[5]Dipartimento di Scienze del Farmaco e della Salute,
Università degli Studi di Catania,
Viale A. Doria 6, I-95125 Catania,
ITALY

Abstract: - Treatment of biofilm-related infections represents a major challenge in public health management. Therefore, the accurate identification of both the composition and architecture of bacterial biofilms, in terms of microorganisms and surrounding extracellular polymeric substances (EPSs), represents a fundamental pre-requisite for the rapid diagnosis of recurrent/resistant biofilm-based infections as well as for the management of several industrial processes. In this work, the results of a combined approach involving scanning electron microscopy (SEM), Fourier-transform infrared spectroscopy in attenuated total reflectance geometry (FTIR-ATR) and μ-Raman spectroscopy for the morphological and physicochemical characterization of monomicrobial biofilms produced by *Pseudomonas aeruginosa* (PAO1) and *Escherichia coli* strains, both proficient in infecting human cells and in colonizing medical devices, are presented. In particular, SEM images revealed, for both producing strains, the presence of densely aggregated rod-shaped bacteria on the surface of an extracellular matrix characterized by a "tree trunk"-like matrix, in the case of PAO1, and a "stone"-like one for *E. coli*, respectively. In addition, several *markers* based on FTIR-ATR and μ-Raman spectral features were identified starting from assessing the biochemical content of both investigated biofilms. In particular, absorption and scattering features associated with the genetic content turned out to be suitable *markers* for the proper discrimination between the PAO1 and *E. coli* biofilm samples, extremely useful in the context of specific therapeutic scheme to be applied. A further aim of this study was the implementation and development

1 Introduction

Biofilms are complex microbial communities embedded in a self-produced matrix that consists of extracellular polymeric substances (EPS), such as polysaccharides, proteins, external DNA (eDNA), lipids, and water. The composition of the EPS varies considerably depending on the producing microbial species and its production is related to the specific environmental conditions including the availability of nutrients, temperature, and oxygen levels, [1], [2]. The resulting structure provides a protective environment for bacterial cells favoring their survival by protecting the enclosed microorganisms from the external environment, antimicrobial agents, and the host's immune defenses.

According to the *National Institutes of Health*, 70% of all human microbial infections stem from biofilms. These infections contribute to a wide range of diseases, including non-healing chronic wounds, endocarditis, periodontitis, cystic fibrosis, rhinosinusitis, meningitis, osteomyelitis, kidney infections, ocular infections, and the infections associated with prostheses and implantable devices. The great clinical significance of biofilm-associated infections and their inherent recalcitrance to antibiotic treatment urgently demanded the development of novel anti-biofilm strategies. In this sense, the development of systems capable of preventing/breaking/dissolving biofilm-associated infections cannot ignore a deep knowledge of several factors including the spatial distribution of cells and extracellular substances, precise identification of the biochemical constitution of microbial species, and physicochemical interactions existing between the different biofilm components.

Currently, biofilm characterization tools typically involve a combination of microscopic, spectroscopic, and molecular techniques, [3], [4], [5], [6], [7]. In particular, microscopy was one of the pioneering approaches utilized to explore biofilm structures and architectures. Arrangements of such complex systems on a solid surface were, in fact, deeply examined with scanning electron microscopy (SEM) and transmission electron microscopy (TEM) [8], [9], while confocal laser scanning (CLSM) or atomic force microscopy (AFM) revealed useful for monitoring biofilm structure during the accumulation stage [10], [11]. More recently, the pioneering breakthrough in 3D imaging of biofilms following the advent of X-ray microtomography (XT) resulted in the possibility of obtaining three-dimensional biofilm images within porous media. To address the issue related to the remarkably similar X-ray absorption coefficients between the aqueous phase and biofilm components, the employment of neutrons, owing to their differential sensitivity towards H and D, represents a good strategy to study the structure and behavior of asymmetric membranes [12], as recently reported in [13].

In addition to the aforementioned techniques, vibrational spectroscopies, such as IR absorption and Raman scattering, have been largely used to achieve a non-invasive molecular characterization of the biofilm composition, [14], [15], [16], [17], [18]. However, considering that spectral profiles of different bacteria are quite similar, the identification of their chemical constituents when embedded in a large class of molecules including carbohydrates, lipids, proteins, and genetic constituents (DNA/RNA), represents a complex and challenging task, [19], [20], [21]. In fact, slight shifts and dissimilarities in peak intensities registered in both IR and Raman spectra can be related to differences in the biofilm biochemistry, thus allowing the characterization and discrimination of the biochemical constitution of the main microbial species, [22]. In [23], authors were the first to establish a rapid identification approach for pathogenic bacteria of clinical isolates by means of Fourier-transform infrared spectroscopy (FTIR) analysis. On the other side, in [24], near-infrared Raman spectroscopy was employed to detect pathogens present in the bloodstream of hospitalized patients suffering from infections, while in [25] dispersive Raman spectroscopy to classify 38

clinical strains from 7 bacterial species was utilized, proving a 100% chance of distinguishing between Gram-positive and Gram-negative bacteria.

In this context, the present study was aimed at evaluating the morphological and physicochemical properties of two different monomicrobial biofilms produced by *Pseudomonas aeruginosa* (PAO1) and *Escherichia coli* (*E. coli*) bacterial strains (Gram-negative species), both capable of infecting human cells or colonizing medical devices, and frequently associated with hospital-acquired infections and mortality worldwide. The combination of scanning electron microscopy (SEM), Fourier-transform infrared spectroscopy in attenuated total reflectance geometry (FTIR-ATR), and μ-Raman techniques proves to be useful for the assessment of the different cell morphology as well as for the identification and analysis of their composition in terms of nucleic acids, carbohydrates, proteins, and extracellular polymeric substances, with the aim to retrieve *smart markers* for their fast and reliable discrimination.

Such preliminary investigation falls within the scope of the PRIN 2022 *FINI* (Future challenges in management of recurrent/resistant Infection: development of antimicrobial Nanoparticulate systems and physical-chemical investigation of their Interactions with biofilm-associated infection) project, funded by the European Union - *Next Generation EU*, focused on the development of novel anti-biofilm strategies based on innovative antimicrobial nanoparticles (NPs) able to eradicate biofilm-associated infections.

2   Materials and Methods

2.1   Materials

2.1.1 Bacterial Strains
In this study, we examined the biofilm formation of *Pseudomonas aeruginosa* strain PAO1 (ATCC 15692) and *E. coli* (strain ATCC 35218), both Gram-negative species. These strains were purchased from the American Type Culture Collection (Rockville, MD, USA).

2.1.2 Biofilm Formation
PAO1 and *E. coli* ATCC 35218 biofilms were developed statically and aerobically in polystyrene 6-well cell culture plates.

Briefly, the bacterial suspensions grown overnight in Luria Bertani broth (LB) (Oxoid, Thermo Fisher Scientific, Waltham, MA, USA) were adjusted in fresh LB medium to a turbidity of

0,5 McFarland standard ($1,5 \times 10^8$ CFU/mL), validated by viable counts on Luria Bertani Agar plates (LB agar) (Oxoid, Thermo Fisher Scientific, Waltham, MA, USA). Then, 6 ml of these suspensions were placed in each polystyrene 6-well flat-bottom cell culture plate (Corning, USA) and statically incubated for 7 days to allow biofilm formation at the bottom of the wells. After incubation, the medium was gently aspirated, and the wells were rinsed twice with phosphate-buffered saline solution (PBS) to remove planktonic cells. Finally, the plate was air-dried for 2 h to be subjected to the different biofilm characterization methods.

2.2   Experimental Methods

2.2.1 Scanning Electron Microscopy (SEM)
For SEM analyses, the two different monospecies biofilms were grown at the bottom of the polystyrene 6-well cell culture plates as described in *section 2.1.2*. Subsequently, the dry biofilm samples were fixed using 1% glutaraldehyde v/v in PBS for 10 minutes and post-fixed in OsO4 1% solution in PBS for 60 minutes. Finally, the samples were air-dried, mounted on an aluminum specimen holder, and sputter-coated with a thin film of gold through a sputtering process performed with an Agar Sputter Coater AGB7340 machine (Assing, Italy). The SEM images were acquired at two different magnifications (500 X and 3000 X), using a SEM EVO 15 (Zeiss, Cambridge, UK), equipped with a LaB$_6$ (Lanthanum Hexaboride) emitter as an electron source. For these morphological analyses, the working distance (WD) was varied from 11,5 up to 14 mm, while electron high tension (ETH) was set at 20 kV.

2.2.2   FTIR-ATR Measurements
Fourier-transform infrared spectroscopy in attenuated total reflectance geometry (FTIR-ATR) spectra were acquired through a FT-IR iS50 Nicolet Thermo Scientific spectrometer equipped with an ATR diamond window module, in the middle infrared range (from 4000 cm^{-1} to 400 cm^{-1}), accumulating 32 scans, with a spectral resolution of 4 cm^{-1}.

2.2.3   μ-Raman measurements
μ-Raman measurements were performed with an iHR550 HORIBA spectrometer, by using a 473 nm excitation wavelength and a Syncerity CCD detector, combined with a BX51 Olympus microscope (grating 600 l/mm).

3 Results and Discussion

Scanning electron microscopy images of the biofilm matrix produced by PAO1 and *E. coli* are shown in Figure 1a-d. The analysis of the shape of the microorganisms and their relative organization, with respect to other microbes and to the EPS matrix, revealed for both PAO1 and *E. coli*, the presence of rod-shaped bacteria aggregated at the surface of a morphologically variable extracellular matrix, depending on the producing strain.

SEM images at 0.5 *k* magnification provided a panoramic view of the spread of the 2 different monomicrobial biofilms (light grey areas) on the surface of the colonized polystyrene well (dark grey area). In detail, through these images at lower magnification, it was possible to observe the presence, on the examined surface, of numerous filamentous structures in the case of PAO1 (Figure 1a) and of densely connected granular structures in the case of *E. coli* (Figure 1c). Instead, higher magnification images allowed us to highlight structural details of the overall architecture of the two bacterial biofilms revealing, in the case of PAO1, the presence of uncovered bacilli surrounded by a structure similar to a "tree trunk", most likely representing their matrix, composed mainly of a thick and dense, layer of alginate (Figure 1b). On the contrary, higher magnification images of the *E. coli* biofilm showed isolated bacteria and "stone"-like clusters of rod-shaped microbes surrounded by a dense extracellular matrix (Figure 1d).
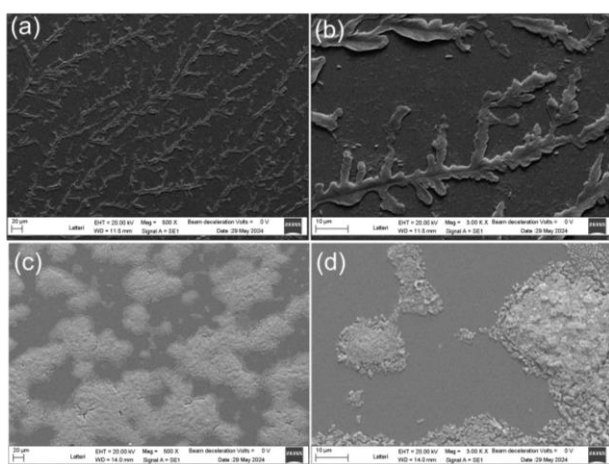

Fig. 1: SEM images of the (a,b) PAO1 and (c,d) E. coli biofilm with 0.5 and 3.0 k magnifications, respectively

Figure 2 reports the comparison between the experimental FTIR-ATR spectra of the investigated PAO1 and *E. coli* biofilm samples in the wavenumber range between 800 cm^{-1} and 4000 cm^{-1}. From a first inspection of the figure, obtained FTIR-ATR spectra appear rather similar with strong absorptions in the regions assignable for polysaccharides/nucleic acids (900-1250 cm^{-1}), proteins (1250 – 1700 cm^{-1}) lipids (2800 – 3000 cm^{-1}) and water (3100 – 3700 cm^{-1}) [26], [27].
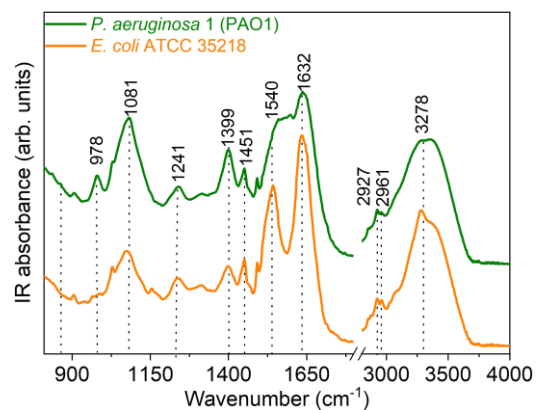

Fig. 2: FTIR-ATR of PAO1 and E. coli biofilm samples in the wavenumber range between 800 cm^{-1} and 4000 cm^{-1}. Spectra were vertically offset for clarity

More in detail, the absorption peak centered at ~ 978 cm^{-1} can be attributed to the backbone C-O and C-C stretching modes of RNA and DNA of the self-produced matrix, [14], [28], [29]. The observation of such a feature only in PAO1 indicates a higher content of such genetic material with respect to *E. coli*, representing a good marker for biofilm discrimination. Then, contributions falling at ~ 1081 cm^{-1} and ~ 1241 cm^{-1} can be attributed, respectively, to the symmetric and antisymmetric phosphate PO$_2^-$ stretching modes of nucleic acids, and also contribute to the asymmetric C-O-C stretching vibration of aliphatic esters and different oligo- and poly-saccharides, [30], [31], [32], [33].

Going on, the 1250–1700 cm^{-1} wavenumber range holds stretching and bending vibrations associated with the –CH$_3$, C–N, N–H and C=O bonds of methyl, amide II, and amide I groups of proteins, respectively falling at ~ 1399 cm^{-1}, ~ 1540 cm^{-1} and ~ 1632 cm^{-1}, [28], [29], [34]. Besides the molecular signature of proteins and the biological nature of the fouling layer, the 1250–1700 cm^{-1} range also includes the asymmetric –CH$_3$ bending vibration of the methyl groups of lipids (~ 1451 cm^{-1}) [29], whose position can reflect variations in membrane fluidity as well as lipid packing, both related to the biofilm's physiological state and susceptibility to different environmental stresses. Noteworthy, the observation of two well-structured amide absorption bands, as in the case of *E. coli* (see the orange profile in Figure 2), could be considered an indication of the existence of a planktonic phase

or of a biofilm at the early stage of development, [35]. However, in our case, considering that both spectra were collected from one-week mature biofilms grown on a polystyrene slide, the observed difference in the amide absorption features between the investigated biofilms denotes a completely different arrangement of the protein structure. In particular, in the case of PAO1, for which a merge of the amide I and amide II absorption bands can be observed, different protein secondary forms of the alpha-helix- and beta-sheet-type, with possible higher degree of conformational diversity, can be hypothesized, in turn suggesting alterations in protein folding or denaturation within the biofilm.

The asymmetric C-H stretching vibrations of both –CH_2 and –CH_3 functional groups of lipids and fatty acids give rise to the absorption peaks falling at ~ 2927 cm^{-1} and ~ 2961 cm^{-1} [26], [28], characteristic of bacterial cell walls and membranes. The slight dissimilarity in the relative intensities between the aforementioned features in PAO1 and *E. coli* biofilm samples, suggests a different lipid nature of the bacterial membranes within the investigated strains. In fact, in the case of the PAO1 biofilm sample, the slightly higher intensity of the absorption feature falling at ~ 2927 cm^{-1} with respect to the one at ~ 2961 cm^{-1}, could reflect a higher proportion of methylene groups with respect to methyl ones, indicating longer and/or more saturated fatty acid chains. Conversely, the comparable intensities of such features in the case of the *E. coli* sample indicate branched fatty acid chains accompanied by structural differences in the lipid composition.

Finally, the large band in the 3100–3600 cm^{-1} wavenumber region accounts, mostly, for the O–H stretching vibrations of hydroxyl groups of water and other biofilm components, which appeared to be almost overlapped with the N–H stretching vibrations of proteins and polysaccharides, [26], [28]. In our samples, hydroxyl moieties mainly originate from water molecules entrapped within the EPS matrix, as well as from the presence of OH residues from polysaccharides, proteins, lipids, and eDNA. Moreover, the slight dissimilarities observed in the O–H stretching region between the investigated biofilm samples could also be reasonably ascribed to the presence of different populations of OH oscillators present in the system, reflecting, in turn, different H-bonded water molecules embedded within the structure. In particular, considering the general idea that the low and high-frequency sides of the 3100–3600 cm^{-1} are respectively attributed to strong and weak hydrogen-bonded OH features [36], an over-population of

highly interconnected water molecules, exhibiting strong H-bonds on both the hydrogen atoms, can be observed in the *E. coli* sample with respect to the PAO1, constituting another bio-marker for proper discrimination. It is worth noting that the presence of bounded water molecules can aid the adhesiveness of the EPS matrix and contribute to the barrier function of bacterial membranes, [37].

With the aim to provide further relevant information in terms of molecular composition and highlight new possible *smart marker* for bacterial recognition, Figure 3 reports the comparison of the μ-Raman spectra of PAO1 and *E. coli* biofilm samples in the wavenumber range between 400 cm^{-1} and 1800 cm^{-1}.
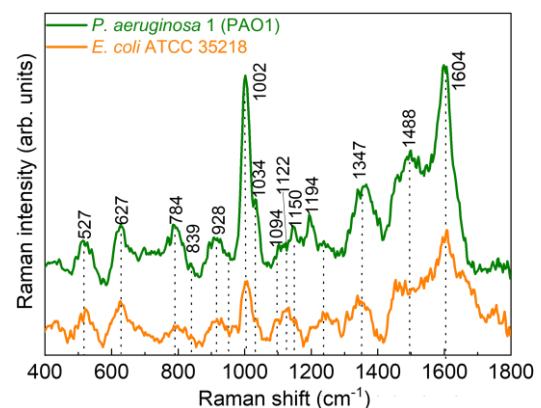

Fig. 3: μ-Raman spectra of PAO1 and E. coli biofilm samples in the wavenumber range between 400 cm^{-1} and 1800 cm^{-1}. Spectra were vertically offset for clarity

As can be seen from the obtained profiles, the general similarity between the spectra of the different species suggests a common biochemical composition, as already evidenced by FTIR-ATR. More in detail, contribution centered at ~ 527 cm^{-1} could be ascribed to the C-O-C glycosidic ring deformation and skeletal modes of glucosamine and *N*-acetyl glucosamine (NAG) [22], while the Raman feature centered at ~ 627 cm^{-1} can be assigned to the presence of phenylalanine (protein), suggesting the presence of enzyme phenylalanine deaminase in both microorganisms, [22].

Then, the Raman band at ~ 784 cm^{-1} corresponds to the bacterial genetic content, *i.e.* DNA and RNA, which appear to be more pronounced in PAO1 with respect to *E. coli*, reflecting, as expected, its higher genome and RNA content and thus its potentially greater transcriptional activity. Furthermore, bands at ~ 839 cm^{-1}, ~ 928 cm^{-1}, ~ 1002 cm^{-1} and ~ 1034 cm^{-1} could be ascribed to the C-C stretching vibrations of tyrosine (~ 839 cm^{-1}, observable only in PAO1) and Amide III groups (~ 928 cm^{-1}), C–C

Giuseppe Paladini,
Francesco Caridi, Domenico Majolino et al.

skeletal stretching of phenylalanine aromatic rings (~ 1002 cm^{-1}) and C–H in-plane deformations of phenylalanine/proline proteins (~ 1034 cm^{-1}), respectively, [38]. Interestingly, only for the *E. coli* biofilm, the presence of two contributions centered at ~ 1094 cm^{-1} and ~ 1122 cm^{-1} assigned, respectively, to the symmetric phosphate PO$_2^-$ stretching modes of nucleic acids and C–C/C–O–C skeletal stretching of saccharides (~ 1094 cm^{-1}), and the C–N/C–C stretching of amide/acyl backbone in lipids ~ 1122 cm^{-1}), can be distinguished. At the same time, a couple of spectral features falling at ~ 1150 cm^{-1} and ~ 1194 cm^{-1} can be observed only in the case of PAO1, accounting for the C–C stretching of carotenoids and C–H wagging of tyrosine, guanine and cytosine. The composition of the PAO1 biofilm appears, once again, rich in nucleic acids supporting the hypothesis of a predominant spontaneous cell lysis with respect to *E. coli*. Such a phenomenon might also reflect an adaptive response to environmental stresses or a strategy to enhance nutrient availability and recycling within the biofilm. In addition, the presence of high amount of nucleic acids could also derive from processes of active secretion, which play a key role in biofilm formation and development. It is worth noting that the importance of genomic material and extracellular DNA in the formation of biofilms of *Pseudomonas* species has already been demonstrated by other authors, [39], [40], [41].

Finally, bands at ~ 1347 cm^{-1}, 1488 cm^{-1} and 1604 cm^{-1} could be assigned, respectively, to the N–H stretching mode of amide III as well as to the bending vibrations of the –CH$_2$ and –CH$_3$ groups in fatty acids [14] (~ 1347 cm^{-1}), ring stretching of adenine [38] (a purine nitrogen base), and to the C=O stretching of amide I groups of proteins, [42].

From the whole set of results, the different bacterial genetic contents turned out to be, rather than other factors, the main responsible for the dissimilarities observed in both the FTIR-ATR and μ-Raman profiles of the PAO1 and *E. coli* biofilm. Absorption and scattering features associated with genetic material can thus be considered good *markers* for the fast discrimination of investigated bacterial strains, extremely useful in the context of specific therapeutic schemes to be implemented, thereby reducing the reliance on empirical antibiotic therapy.

4 Conclusion

In this paper, a preliminary morphological and physicochemical investigation of two different bacterial biofilms produced by PAO1 and *E. coli* strains was carried out through a combination of SEM, FTIR-ATR, and μ-Raman spectroscopy techniques. In particular, SEM analysis allowed the possibility to highlight the shape of the microorganisms composing the biofilm and their organization relative to other bacteria and to the self-produced extracellular matrix. Furthermore, the assessment of the chaotic molecular composition of investigated biofilms, in conjunction with the accurate recognition of each spectral dissimilarity observed between the two samples, allowed us to identify specific biochemical *smart markers* for fast and reliable biofilm discrimination. Obtained results not only furnish a better understanding of the complex nature of the biofilm architecture supporting, at the same time, the development of an even more accurate database for FTIR-ATR and μ-Raman band assignments but also would provide crucial information to design optimized nanotechnological systems for the management of recurrent/resistant biofilm-based infections.

References:
[1] M.K. Mosharaf, M.Z.H. Tanvir, M.M. Haque, M.A. Haque, M.A.A. Khan, A.H. Molla, M.Z. Alam, M.S. Islam, M.R. Talukder, Metal-adapted bacteria isolated from wastewaters produce biofilms by expressing proteinaceous curli fimbriae and cellulose nanofibers, *Frontiers in Microbiology*, Vol. 9, 2018, p.1334. DOI: 10.3389/fmicb.2018.01334.

[2] B. a Annous, P.M. Fratamico, J.L. Smith, Quorum Sensing in Biogilms: Why Bacteria Behave the Way They Do, *Journal of Food Science*, Vol.74, 2009, pp.1–15. DOI: 10.1111/j.1750-3841.2008.01022.x.

[3] S. Keleştemur, E. Avci, M. Çulha, Raman and Surface-Enhanced Raman Scattering for Biofilm Characterization, *Chemosensors*, Vol.6, 2018, p.5. DOI: 10.3390/chemosensors6010005.

[4] R. Funari, A.Q. Shen, Detection and Characterization of Bacterial Biofilms and Biofilm-Based Sensors, *ACS Sensors*, Vol.7, 2022, pp.347–357. DOI: 10.1021/acssensors.1c02722.

[5] Y. Zhang, P. Young, D. Traini, M. Li, H.X. Ong, S. Cheng, Challenges and current advances in in vitro biofilm characterization, *Biotechnology Journal*, Vol.18, 2023, p. 2300074. DOI: 10.1002/biot.202300074.

[6] D. Chirman, N. Pleshko, Characterization of

bacterial biofilm infections with Fourier transform infrared spectroscopy: a review, *Applied Spectroscopy Reviews*, Vol.56, 2021, pp.673–701. DOI: 10.1080/05704928.2020.1864392.

[7] M.C. Sportelli, C. Kranz, B. Mizaikoff, N. Cioffi, Recent advances on the spectroscopic characterization of microbial biofilms: A critical review, *Analytica Chimica Acta*, Vol.1195, 2022, p.339433. DOI: 10.1016/j.aca.2022.339433.

[8] O. Nwaiwu, L. Wong, M. Lad, T. Foster, W. MacNaughtan, C. Rees, Properties of the Extracellular Polymeric Substance Layer from Minimally Grown Planktonic Cells of Listeria monocytogenes, *Biomolecules*, Vol.11, 2021, p.331. DOI: 10.3390/biom11020331.

[9] J. McCutcheon, G. Southam, Advanced biofilm staining techniques for TEM and SEM in geomicrobiology: Implications for visualizing EPS architecture, mineral nucleation, and microfossil generation, *Chemical Geology*, Vol. 498, 2018, pp. 115-127. DOI: 10.1016/j.chemgeo.2018.09.016.

[10] M.J. Franklin, C. Chang, T. Akiyama, B. Bothner, New Technologies for Studying Biofilms, *Microbiology Spectrum*, Vol.3, 2015, pp.1–23. DOI: 10.1128/microbiolspec.MB-0016-2014

[11] N.H. Faiq, M.E. Ahmed, Inhibitory Effects of Biosynthesized Copper Nanoparticles on Biofilm Formation of Proteus mirabilis, *Iraqi Journal of Science*, Vol.65, 2024, pp.65–78. DOI: 10.24996/ijs.2024.64.1.7.

[12] N. Paracini, L.A. Clifton, J.H. Lakey, Studying the surfaces of bacteria using neutron scattering: finding new openings for antibiotics, *Biochemical Society Transactions*, Vol.48, 2020, pp.2139–2149. DOI: 10.1042/BST20200320.

[13] S. Rolland du Roscoat, T. Ivankovic, N. Lenoir, S. Dekic, J.M.F. Martins, C. Geindreau, First visualisation of bacterial biofilms in 3D porous media with neutron microtomography without contrast agent, *Journal of Microscopy*, Vol.285, 2022, pp.20–28. DOI: 10.1111/jmi.13063.

[14] B. Gieroba, M. Krysa, K. Wojtowicz, A. Wiater, M. Pleszczyńska, M. Tomczyk, A. Sroka-Bartnicka, The FT-IR and Raman Spectroscopies as Tools for Biofilm Characterization Created by Cariogenic Streptococci, *International Journal of Molecular Sciences*, Vol.21, 2020, p.3811.

DOI: 10.3390/ijms21113811.

[15] T. Misra, M. Tare, P.N. Jha, Insights Into the Dynamics and Composition of Biofilm Formed by Environmental Isolate of Enterobacter cloacae, *Frontiers in Microbiology*, Vol.13, 2022, p.877060. DOI: 10.3389/fmicb.2022.877060.

[16] A.E.R.R. El Shanshoury, S.Z. Sabae, W.A. El Shouny, H.E. Elsaied, H.M. Badr, A.M. Abo-Shady, Biomimetic Synthesis of Silver Nanoparticles Using New Aquatic Species of Bacillus, Alcaligenes, and Paenibacillus and their Potential Antibiofilm Activity against Biofilm-Forming Escherichia coli, *Letters in Applied NanoBioScience*, Vol.12, 2022, p.127. DOI: 10.33263/LIANBS124.127.

[17] R. Udupa, P. Peralam Yegneswaran, J. Lukose, S. Chidangil, Utilization of Raman spectroscopy for identification and characterization of fungal pathogens, *Fungal Biology Reviews*, Vol.47, 2024, p.100339. DOI: 10.1016/j.fbr.2023.100339.

[18] E. Efeoglu, M. Culha, In Situ-Monitoring of Biofilm Formation by Using Surface-Enhanced Raman Scattering, *Applied Spectroscopy*, Vol.67, 2013, pp.498–505. DOI: 10.1366/12-06896.

[19] L.-P. Choo-Smith, K. Maquelin, T. van Vreeswijk, H.A. Bruining, G.J. Puppels, N.A.N. Thi, C. Kirschner, D. Naumann, D. Ami, A.M. Villa, F. Orsini, S.M. Doglia, H. Lamfarraj, G.D. Sockalingum, M. Manfait, P. Allouch, H.P. Endtz, Investigating Microbial (Micro)colony Heterogeneity by Vibrational Spectroscopy, *Applied and Environmental Microbiology*, Vol.67, 2001, pp.1461–1469.
DOI: 10.1128/AEM.67.4.1461-1469.2001.

[20] L. Zeiri, B. V. Bronk, Y. Shabtai, J. Eichler, S. Efrima, Surface-Enhanced Raman Spectroscopy as a Tool for Probing Specific Biochemical Components in Bacteria, *Applied Spectroscopy*, Vol.58, 2004, pp.33–40. DOI: 10.1366/000370204322729441.

[21] V. Ciobotă, E.-M. Burkhardt, W. Schumacher, P. Rösch, K. Küsel, J. Popp, The influence of intracellular storage material on bacterial identification by means of Raman spectroscopy, *Analytical and Bioanalytical Chemistry*, Vol.397, 2010, pp.2929–2937. DOI: 10.1007/s00216-010-3895-1.

[22] F.S. de Siqueira e Oliveira, A.M. da Silva, M.T.T. Pacheco, H.E. Giana, L. Silveira, Biochemical characterization of pathogenic

bacterial species using Raman spectroscopy and discrimination model based on selected spectral features, *Lasers in Medical Science*, Vol.36, 2021, pp.289–302. DOI: 10.1007/s10103-020-03028-9.

[23] D. Naumann, V. Fijala, H. Labischinski, P. Giesbrecht, The rapid differentiation and identification of pathogenic bacteria using Fourier transform infrared spectroscopic and multivariate statistical analysis, *Journal of Molecular Structure*, Vol.174, 1988, pp.165–170. DOI: 10.1016/0022-2860(88)80152-2.

[24] K. Maquelin, L.-P. Choo-Smith, T. van Vreeswijk, H.P. Endtz, B. Smith, R. Bennett, H.A. Bruining, G.J. Puppels, Raman Spectroscopic Method for Identification of Clinically Relevant Microorganisms Growing on Solid Culture Medium, *Analytical Chemistry*, Vol.72, 2000, pp.12–19. DOI: 10.1021/ac991011h..

[25] F.S. de Siqueira e Oliveira, H.E. Giana, L. Silveira, Discrimination of selected species of pathogenic bacteria using near-infrared Raman spectroscopy and principal components analysis, *Journal of Biomedical Optics*, Vol.17, 2012, p.107004. DOI: 10.1117/1.JBO.17.10.107004.

[26] M. Kardas, A.G. Gozen, F. Severcan, FTIR spectroscopy offers hints towards widespread molecular changes in cobalt-acclimated freshwater bacteria, *Aquatic Toxicology*, Vol.155, 2014, pp.15–23. DOI: 10.1016/j.aquatox.2014.05.027.

[27] S. Cheeseman, Z.L. Shaw, J. Vongsvivut, R.J. Crawford, M.F. Dupont, K.J. Boyce, S. Gangadoo, S.J. Bryant, G. Bryant, D. Cozzolino, J. Chapman, A. Elbourne, V.K. Truong, Analysis of Pathogenic Bacterial and Yeast Biofilms Using the Combination of Synchrotron ATR-FTIR Microspectroscopy and Chemometric Approaches, *Molecules*, Vol.26, 2021, p.3890. DOI: 10.3390/molecules26133890.

[28] E. San-Blas, N. Cubillán, M. Guerra, E. Portillo, I. Esteves, Characterization of Xenorhabdus and Photorhabdus bacteria by Fourier transform mid-infrared spectroscopy with attenuated total reflection (FT-IR/ATR), *Spectrochimica Acta Part A: Molecular and Biomolecular Spectroscopy*, Vol.93, 2012, pp.58–62. DOI: 10.1016/j.saa.2012.03.006.

[29] Z. Movasaghi, S. Rehman, D.I. ur Rehman, Fourier Transform Infrared (FTIR) Spectroscopy of Biological Tissues, *Applied Spectroscopy Reviews*, Vol.43, 2008, pp.134–179. DOI: 10.1080/05704920701829043.

[30] N. Simsek Ozek, I.B. Bal, Y. Sara, R. Onur, F. Severcan, Structural and functional characterization of simvastatin-induced myotoxicity in different skeletal muscles, *Biochimica et Biophysica Acta*, Vol.1840, 2014, pp.406–415. DOI: 10.1016/j.bbagen.2013.09.010.

[31] S. Garip, A.C. Gozen, F. Severcan, Use of Fourier transform infrared spectroscopy for rapid comparative analysis of Bacillus and Micrococcus isolates, *Food Chemistry*, Vol.113, 2009, pp.1301–1307. DOI: 10.1016/j.foodchem.2008.08.063.

[32] G. Cakmak, I. Togan, F. Severcan, 17β-Estradiol induced compositional, structural and functional changes in rainbow trout liver, revealed by FT-IR spectroscopy: A comparative study with nonylphenol, *Aquatic Toxicology*, Vol.77, 2006, pp.53–63. DOI: 10.1016/j.aquatox.2005.10.015.

[33] F. Humbert, F. Quilès, In-situ study of early stages of biofilm formation under different environmental stresses by ATR-FTIR spectroscopy, *Science against Microbial Pathogens: Communicating Current Research and Technological Advances, A. Mendez-Vilas (Eds.)*, 2011.

[34] M.S.I. Khan, E.-J. Lee, Y.-J. Kim, A submerged dielectric barrier discharge plasma inactivation mechanism of biofilms produced by Escherichia coli O157:H7, Cronobacter sakazakii, and Staphylococcus aureus, *Scientific Reports*, Vol.6, 2016, p.37072. DOI: 10.1038/srep37072.

[35] A.R. Crisp, B. Short, L. Rowan, G. Ramage, I.U.R. Rehman, R.D. Short, C. Williams, Investigating the chemical pathway to the formation of a single biofilm using infrared spectroscopy, *Biofilm*, Vol.6, 2023, p.100141. DOI: 10.1016/j.bioflm.2023.100141.

[36] G. Paladini, V. Venuti, V. Crupi, D. Majolino, A. Fiorati, C. Punta, FTIR-ATR analysis of the H-bond network of water in branched polyethyleneimine/TEMPO-oxidized cellulose nano-fiber xerogels, *Cellulose*, Vol.27, 2020, pp.8605–8618. DOI: 10.1007/s10570-020-03380-7.

[37] K. Quan, J. Hou, Z. Zhang, Y. Ren, B.W. Peterson, H.C. Flemming, C. Mayer, H.J. Busscher, H.C. van der Mei, Water in

bacterial biofilms: pores and channels, storage and transport functions, *Critical Reviews in Microbiology*, Vol. 48, 2022, pp.283-302. DOI: 10.1080/1040841X.2021.1962802.

[38] I.H. Boyaci, H.T. Temiz, H.E. Geniş, E. Acar Soykut, N.N. Yazgan, B. Güven, R.S. Uysal, A.G. Bozkurt, K. İlaslan, O. Torun, F.C. Dudak Şeker, Dispersive and FT-Raman spectroscopic methods in food analysis, *RSC Advances*, Vol.5, 2015, pp.56606–56624. DOI: 10.1039/c4ra12463d.

[39] D. Kusić, B. Kampe, A. Ramoji, U. Neugebauer, P. Rösch, J. Popp, Raman spectroscopic differentiation of planktonic bacteria and biofilms, *Analytical and Bioanalytical Chemistry*, Vol.407, 2015, pp.6803–6813. DOI: 10.1007/s00216-015-8851-7.

[40] R.E. Steinberger, P.A. Holden, Extracellular DNA in Single- and Multiple-Species Unsaturated Biofilms, *Applied and Environmental Microbiology*, Vol.71, 2005, pp.5404–5410. DOI: 10.1128/AEM.71.9.5404-5410.2005.

[41] C.B. Whitchurch, T. Tolker-Nielsen, P.C. Ragas, J.S. Mattick, Extracellular DNA Required for Bacterial Biofilm Formation, *Science*, Vol.295, 2002, p.1487. DOI: 10.1126/science.295.5559.1487.

[42] E. Efeoglu, M. Culha, Surface-enhanced raman scattering for biofilm characterization, *Spectroscopy*, 2013, [Online]. http://www.spectroscopyonline.com/surface-enhanced-raman-scattering-biofilm-characterization (Accessed Date: July 1, 2024).

Contribution of Individual Authors to the Creation of a Scientific Article (Ghostwriting Policy)
- Giuseppe Paladini, Francesco Caridi were responsible for FTIR-ATR and μ-Raman data analysis and interpretation and wrote the original manuscript.
- Federica De Gaetano, Rosanna Stancanelli, Silvana Tommasini wrote the original manuscript and aided in interpreting and processing of the whole set of results and contributed to the review and editing of the manuscript.
- Paola Cardiano, Gabriale Lando carried out the experimental FTIR-ATR measurements on investigated biofilm samples.
- Domenico Majolino, Valentina Venuti, Cinzia Anna Ventura, Venerando Pistarà conceived the original idea and were responsible for conceptualization, supervision, design and implementation of the research.
- Barbara Fazio carried out μ-Raman measurements on investigated biofilm samples.
- Cinzia Lombardo, Mario Salmeri produced investigated monomicrobial biofilms, carried out and interpreted SEM measurements.

Conflict of Interest
The authors have no conflicts of interest to declare.